INTERFEROMETRIC PHASE ANALYSIS FOR MONITORING SLOW DEFORMATION PROCESSES

Ramon Hanssen and Stefania Usai

Delft Institute for Earth Oriented Space Research (DEOS)
Delft University of Technology, P.O. Box 5030, 2600 GA, Delft, the Netherlands.
phone: +31 15 2782565, fax: +31 15 2783711

E-mail: hanssen@geo.tudelft.nl

Abstract— **SAR interferometry has proven to be a feasible tool for detecting ground deformations caused by earthquakes or volcano activity. However, the application of the technique for deformation processes which take place on a longer time scale remains difficult for a number of reasons. Limiting factors for monitoring slow deformation processes are mainly temporal decorrelation and atmospheric delay differences within a SAR scene. Especially areas with agricultural activity lose coherence typically within an interval of days, which is too short to unravel the slow deformation rates. The systematical analysis of series of interferograms seems to be the only possibility for extracting feasible subsidence rates from SAR interferometry. In this paper we will give an overview of the possible error sources and propose a method for the analysis of severely decorrelated phase interferograms.**

I. Introduction

The feasibility of differential SAR interferometry for detecting and quantifying deformation is limited by the characteristics of the deformation and the terrain, the time interval between the two or more SAR acquisitions, and a number of additional phase effects, whether or not coherence preserving.

The characteristics of the deformation can be expressed as the size of the displacement in slant range versus the width of the phenomenon. The size of the displacement is limited by the phase noise and the slope/pixel size ratio which should not exceed aliasing criteria. The detectability of a phenomenon with these parameters is dependent on wavelength, pixel posting, image size, and time. However, this relationship is complicated due to the influence of the time interval between the two consecutive SAR acquisitions. For large areas in the world coherence decreases significantly if the epoch between the acquisitions exceeds more than a couple of days. What remains in the interferogram are isolated patches of coherent information which do contain information but can be ambiguous to interpret. The decrease in coherence is referred to as temporal decorrelation. Moreover, the phase interpretation of such an interferogram suffers from additional coherence preserving phase effects, like the influence of the atmosphere and signal penetration differences in the imagery. These cause a coherent bias in the phase measurement. Naturally, additional coherent phase effects can be caused by the interferometric processing, where e.g. orbit inaccuracies and inconsistencies in the applied Digital Elevation Model (DEM) can cause phase variations in the image. In the present work, we will try to give an overview on the different phase effects and study the effects of propagation heterogeneities, penetration change and temporal decorrelation for slow subsidence studies using SAR interferometry. Approaches are being proposed to use preferably all SAR imagery of a study area to subsequently detect coherent phase errors, identify them, and correct for them.

II. The interferometric phase

The phase observation in a SAR image contains the superposition of a number of effects. If we concentrate on the effects which are independent of the SAR and INSAR processing, the first and most important influence is the geometric distance between the antenna and a resolution element at the earths surface. The signal propagation is a second effect that influences the phase: a delay or acceleration of the velocity of the signal yields a bias in the phase observation. A third effect is the reflection depth and the interaction with the surface. The radar signal, dependent on the wavelength and intensity, does not reflect at the geometrical boundary between the soil and the atmosphere, it penetrates the soil to some extent and is influenced by the dielectric characteristics of it. Apart from phase biases due to geometry, propagation and penetration, a fourth influence on the phase of a SAR resolution cell is the arbitrary superposition of single scatterers within the resolution cell. In equation (1) this summation is given for resolution element p and acquisition i (with $i = \{1, 2\}$).

$$\phi_{p,i} = \phi_{geom,i} + \phi_{prop,i} + \phi_{penetr,i} + \phi_{scat,i} \quad (1)$$

$$\Delta\phi_p = \phi_{p,2} - \phi_{p,1} \quad (2)$$

In the interferometric phase image, the interferogram, the phase observations of acquisition 1 and 2, for a specific resolution element are subtracted from each other, as in equation (2). The geometrical difference between both signals conveys information on (relative) height, deformation, orbit aberrations and the choice of the reference surface. For a single resolution element this information is hard to interpret, and especially the relation between adjacent pixels reflects the above mentioned information. Due to this relative character, the absolute propagation delay caused by the atmosphere is not relevant for SAR interferometry. However, propagation delay heterogeneities within the interferogram scene can easily produce phase differences which are hard to discern from e.g. geometrical phase differences due to topography or deformations. For penetration effects the same line of reasoning holds. As long as the

penetration differences in the first SAR image are equal to those in the second one, the effect is cancelled out. Local penetration change in time yields an interferometric phase effect. Finally, the effect of a temporal change of the scatterers in a resolution cell causes decorrelation, resulting in an increase in phase variance, which decreases the reliability of that particular interferometric phase.

III. Propagation heterogeneities

The effect of propagation differences in the interferometric phase is caused by the spatial and temporal variability in the refractive index in the atmosphere. The phase variations caused by this variability are independent from the interferometric configuration. However, if this interferometric phase is processed to a height estimate, the errors in height increase with the height ambiguity. Therefore large baselines can be used to suppress the influence of atmospheric heterogeneities on DEM generation. For deformation maps, the errors are independent of the baseline. Analysing the effects of the atmosphere on SAR interferometry, we can distinguish between the influence of ionosphere and troposphere. In the following we will discuss both propagation effects.

A. Ionospheric propagation

The SAR phase signal is accelerated if the number of free electrons in the ionosphere increases. To estimate the number of free electrons, the ionosphere is modelled as a single layer at a certain effective height. The electron density is now translated to the Total Electron Content (TEC) at this effective height. To achieve reasonable units, one TECU (TEC Unit) is equal to 10^{16} electrons/m^2. The total range of electron activity varies between 0 and approximately 30 TECU, dependent on solar activity, time of day, latitude, and geomagnetic activity.

The ionospheric range error for a two-way SAR signal can be determined in first approximation using the following equation

$$\Delta R = \frac{2K}{f_{SAR}^2}\mathrm{TEC}\cdot\left(1-\left(\frac{r_e\sin\theta}{r_e+h_{sp}}\right)^2\right)^{-\frac{1}{2}} \qquad (3)$$

In this equation, $K = 40.28$ is an empirically determined constant, f_{SAR} is the specific SAR frequency, and the right multiplication factor is the mapping function, which maps the zenith delay to the SAR incidence angle θ, using the earth radius r_e and the height of the single layer h_{sp}. For TECU values between 0 and 30, the range error for a C-band SAR is between 0 and 0.97 meter. As a rule of thumb for repeat pass interferometry, we can therefore say that 1 TECU difference within a SAR image yields approximately one fringe in the interferogram. Note that if the difference in TEC units is equal in both SAR images, both effects are cancelled out in the interferogram.

In figure 1 it is shown how the TEC units vary for a specific time of day. These values are determined using the network of the International GPS Service for Geodynamics (IGS), and are mainly tidal effects (Jungstand 1997)(Williams 1996).

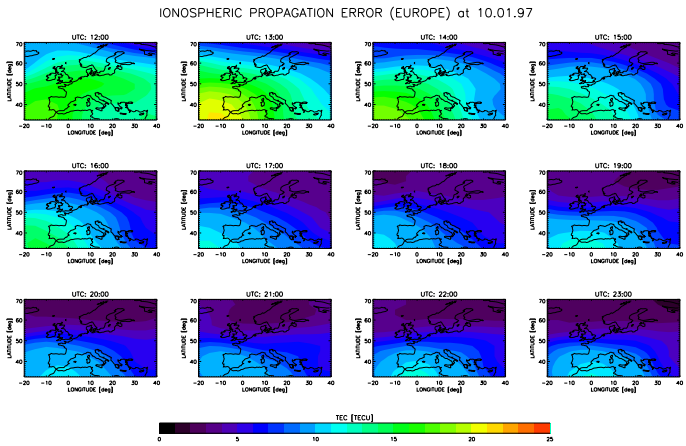

Fig. 1. Example of a hourly map of the Total Electron Content over Europe (Jungstand 1997)

Since the long wavelength features are only causing a small ramp in the interferogram, this ionospheric effect will be hard to recognise and can easily be misinterpreted as an orbit error. Especially if the SAR acquisitions are acquired at the same time of day, it is expected that the effects cancel each other in the interferogram. Travelling Ionospheric Disturbances (TID's), however, are recognised at different spatial wavelengths: large, medium and small, respectively thousands, hundreds and tens of kilometers (Spoelstra 1996),(Williams 1996) and are mainly caused by auroral disturbances which propagate equatorward. Finally small scale ionospheric phenomena, also referred to as acoustic waves (Williams 1996), are characterised as irregularities in the ionosphere's E-region and F-region. Here, nighttime density fluctuations of 10–20% are observed for wavelengths of 30–300m, corresponding with a phase shift of 35–70 degrees. Therefore, ionospheric heterogeneities can be a disturbing influence for SAR interferograms.

B. Tropospheric propagation

The propagation velocity in the troposphere is determined by the refractive index, which is dependent of temperature, pressure and relative humidity. The incremental path length compared to the propagation in vacuum can be determined integrating these parameters over the total path length in the troposphere. The Smith-Weintraub approximation, which is accurate to about 0.5% yields (Smith, Jr. and Weintraub 1953):

$$\Delta\rho = 7.76\cdot10^{-5}\int_0^{top}\frac{P}{T}dx + 3.73\cdot10^{-1}\int_0^{top}\frac{e}{T^2}dx \qquad (4)$$

where P is the total pressure, T is the absolute temperature, and e is the partial pressure of water vapour, which is related to the relative humidity rh with

$$e = \frac{rh}{100}\exp\left(-37.2465+0.213166T-0.000256908T^2\right). \qquad (5)$$

The first term in equation 4 is referred to as the hydrostatic term, which can be relatively well determined using

surface measurements. The evaluation of the second term, however, imposes severe problems due to the high spatial and temporal variability of the relative humidity, especially in the atmospheric boundary layer (the first 1.5 kilometers) and in cloud layers. Although in terms of absolute delay the hydrostatic term accounts for about 90% of the delay, the relative character of the SAR phase observations is mainly sensitive for the variations of the second, 'wet', term (Hanssen and Feijt 1996).

Since cloud cover can be an indication for variations in relative humidity, the interferometric effect of different types of cloud layers is shown in the figures 2, 3, and 4. Figure 2 represents a tandem interferogram of a relatively stable atmosphere with homogeneously distributed cloud cover for both acquisition dates. At the right side of the image, some diagonal internal or gravity waves are visible. In a current study, the atmospheric conditions within this epoch are additionally examined using a local GPS network. In figure 3, the effect of a frontal zone is visible as a diagonal feature in the interferogram. In Hanssen and Feijt (1996), these data were compared with additional surface and satellite meteorological data, which confirmed the hypothesis of a tropospheric change in humidity connected with a frontal zone. Finally, figure 4 shows the effect of convective cells on the interferometric phase. Up to two fringes phase difference are visible, which indicates the presence of convective phenomena with an associated change in humidity characteristics.

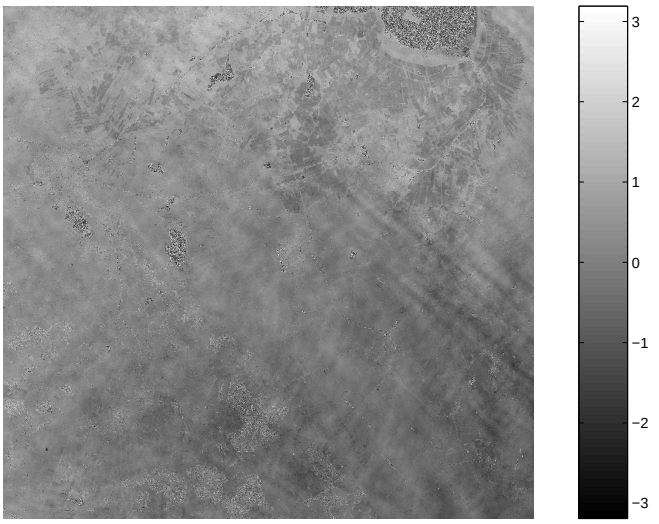

Fig. 2. The effect of internal gravity waves in a homogeneously cloudy troposphere on the interferometric phase

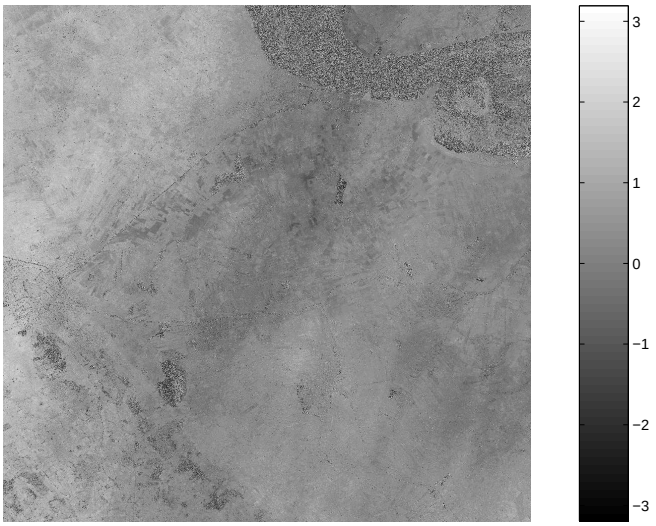

Fig. 3. The effect of a meteorological frontal zone on the interferometric phase

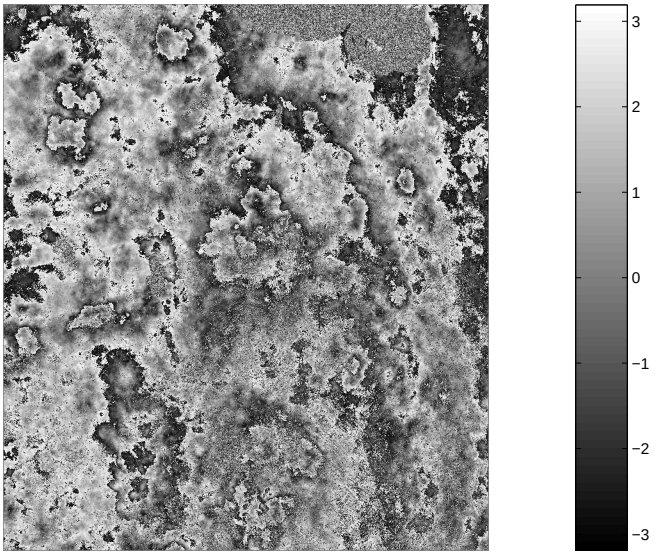

Fig. 4. The effect of convective cells on the interferometric phase

IV. Penetration differences

A coherent change in penetration difference between different types of soil can yield localised phase biases in the interferogram. In figure 5 it is shown how a coherent phase bias of approximately 0.15 phase cycles (corresponding with 5 mm path length change), acts on specific areas in the interferogram which are clearly correlated with areas of different land use. The interferogram is based on a tandem SAR image pair. A change in the dielectric properties of the soil influences the Fresnel reflection coefficient which might yield a coherent phase effect. Another possibility would be a height change due to the expansion of the entire field as a reaction on a localised change in the fields water content (Gabriel, Goldstein, and Zebker 1989). However, since temperature, pressure, relative humidity, wind speed and cloud cover had identical characteristics at both SAR acquisitions and no watering took place in this period, it is considered unlikely that expansion effects dominate for this phase change. Changes in penetration or in the dielectric constant seem to be more likely, although unambiguous interpretation of the effects is difficult without a priori information. If a penetration error propagates in a height estimate, with this effective baseline of 25 meter, an error of 48 meters can be reached when comparing two

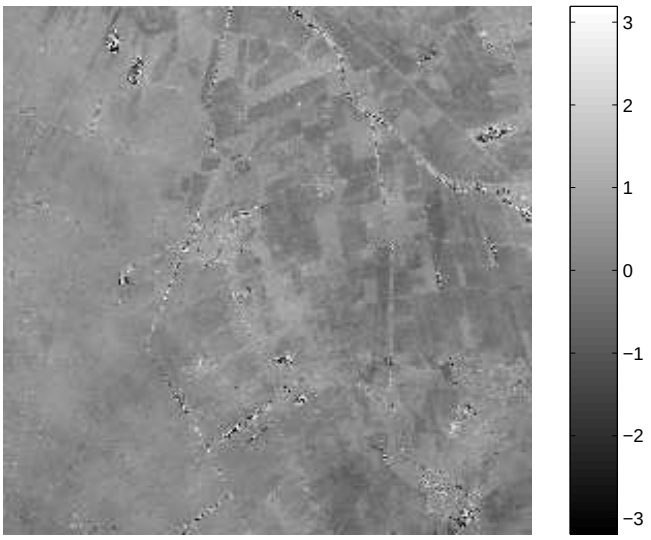

Fig. 5. A 5×5 km zoom of an interferogram showing penetration differences

isolated positions.

V. Temporal decorrelation

In figure 6 it is shown how the coherence over a specific area has decreased over a time interval of 3.5 years. From this coherence image it may seem that no significant information can be retrieved in this interval, since the overall tone of the image has a constant and low value. On the other hand one might conclude that this average coherence value of approximately 0.3 is still interpretable in terms of a reasonable stable interferometric phase. After closer analysis of the data, isolated points with a relatively high coherence estimation can be detected.

As described by Touzi, Lopes, and Vachon (1996), the discrimination between areas of different coherence is mainly influenced by the number of independent samples in the coherence estimation window. If this number is chosen too small, low coherence areas become biased towards a higher coherence estimation. Figure 6, for which an estimation window of 2×11 samples was used, displays this effect—although almost all coherence in this (mostly agricultural) area has disappeared, a bias of approximately 0.3 is apparent in the data. Therefore discrimination between different coherence levels becomes difficult.

As shown in figure 7, an increase of the coherence estimation window to 20×110 samples yields an increased discrimination between areas of different coherence, which is due to the corresponding drop in coherence bias. In the figure, this can be observed in the red tone of the decorrelated areas[1]. On the other hand, areas with a relatively higher coherence can be detected as the yellow and green spots. Naturally, the larger estimation window implies a decrease in the absolute coherence levels with respect to

[1]Note that although a continuous colour wheel proved to be the best visualisation for these data, coherence levels above 0.95 which are also coloured red can be neglected with this estimation window.

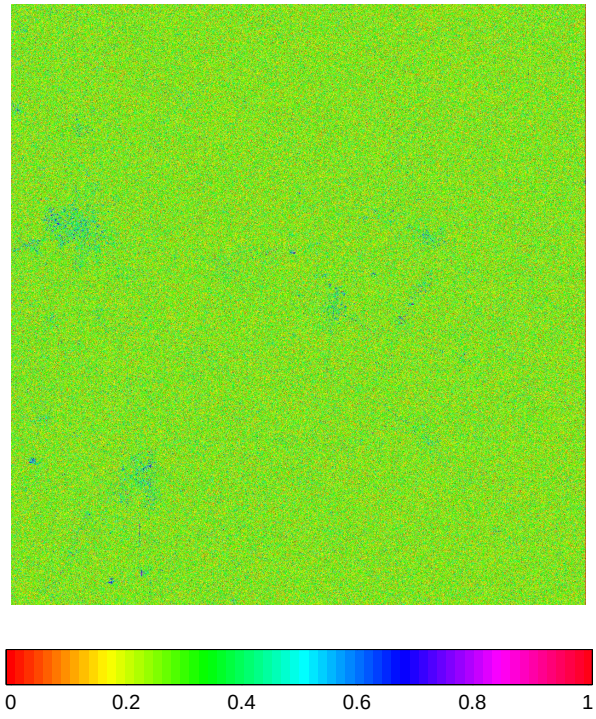

Fig. 6. Coherence image after a 3.5 year time interval, using 2×11 independent samples for the coherence estimation

those of small window sizes. Therefore, the range of coherence values in the image reduces, whereas the reliability of the estimates increases.

Due to the better possibilities to discriminate between coherence levels, thresholding at a chosen low level becomes possible. Figure 8 shows how the interferometric phase values corresponding with pixels with a coherence higher than 0.1 still reveal interpretable phase information. In this masked interferogram, a multilook window equal to the coherence estimation window (20×110) was applied. Although disturbing influences of the satellite orbits or atmospheric heterogeneities still form a major restriction for an unambiguous interpretation, this method of phase analysis reveals promising prospects for the study of long time interval and severely decorrelated interferograms. The coherence preserving areas are in this case mainly of anthropogenic origin.

VI. Conclusions

Phase bias effects due to atmospheric heterogeneities and local temporal penetration differences hamper an unambiguous interpretation of the interferometric phase in terms of geometric path length differences. For slow deformation processes, the need to use interferometric pairs over long time intervals introduces decorrelation effects, which results in an increased phase noise for major parts of the interferogram. Using large coherence estimation windows, the coherence bias is suppressed. This enables the discrimination of different low coherence levels, and the extraction of useful phase information. Finally, strong multilooking reduces the phase variance for the selected parts of the in-

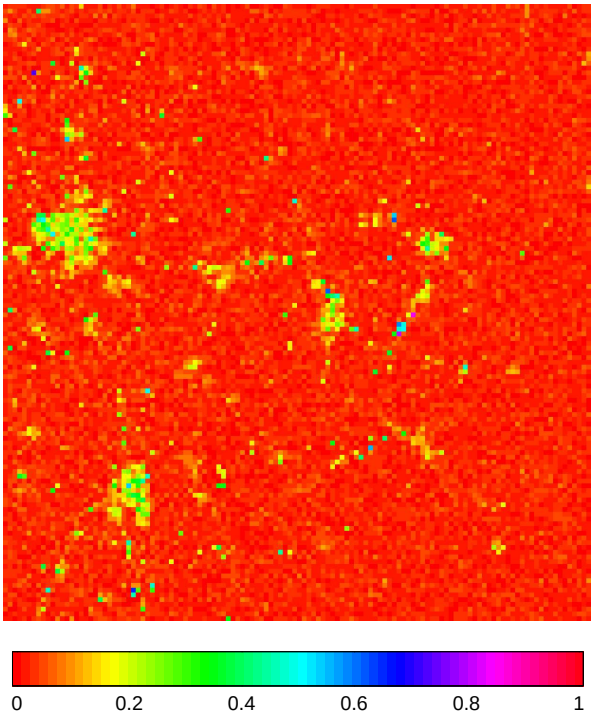

Fig. 7. Coherence image using 20×110 independent samples per pixel

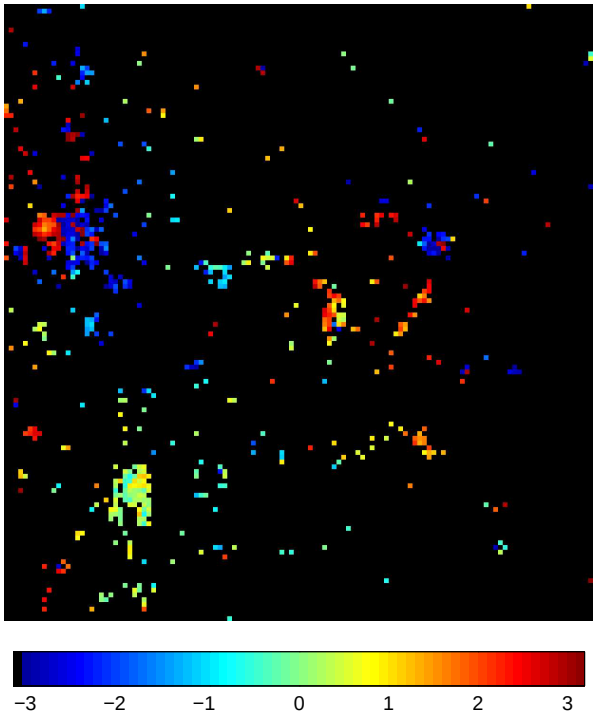

Fig. 8. Interferogram, masked under a coherence level of 0.1 with a multilook window of 20×110 pixels

terferogram.

VII. Acknowledgements

The authors would like to thank the European Space Agency for the provision of the SAR data, and dr. A. Jungstand from DLR Neustrelitz for the kind provision of the ionospheric maps over Europe. Also the support of the group of dr. R.Bamler from DLR Oberpfaffenhofen is kindly appreciated.

References

Gabriel, A. K., R. M. Goldstein, and H. A. Zebker (1989). Mapping small elevation changes over large areas, differential radar interferometry. *Journal of Geophysical Research 94*(B7), 9183–9191.

Hanssen, R. and A. Feijt (1996). A first quantitative evaluation of atmospheric effects on SAR interferometry. In *Fringe workshop Zurich*, http://www.geo.unizh.ch/rsl/fringe96/papers/hanssen/. ESA.

Jungstand, A. (1997). Ionospheric maps and GPS satellite and receiver biases. http://www.nz.dlr.de/gps/gps-ion.html. DLR Remote Sensing Ground Station Neustrelitz.

Kohl, H., R. Rüster, and K. Schlegel (Eds.) (1996). *Modern Ionospheric Science*. Katlenburg-Lindau, FRG: European Geophysical Society.

Smith, Jr., E. K. and S. Weintraub (1953). The constants in the equation for atmospheric refractive index at radio frequencies. *Proceedings of the I.R.E* (41), 1035–1037.

Spoelstra, T. A. T. (1996). A climatology of quiet/disturbed ionospheric conditions derived from 22 years of Westerbork interferometer observations. *Journal of Atmospheric and Terrestrial Physics 58*(11), 1229–1258.

Touzi, R., A. Lopes, and P. W. Vachon (1996). Estimation of the coherence function for interferometric SAR applications. In *EUSAR'96, Königswinter, Germany*, pp. 241–244.

Williams, P. J. S. (1996). *Tides, Atmospheric Gravity Waves and Travelling Disturbances in the Ionosphere*, pp. 136–180. In Kohl et al. Kohl, Rüster, and Schlegel (1996).